Physics of the Solid State, Vol. 46, No. 5, 2004, pp. 969–974. Translated from Fizika Tverdogo Tela, Vol. 46, No. 5, 2004, pp. 938–944.

LOW-DIMENSIONAL SYSTEMS AND SURFACE PHYSICS

Electron-Beam-Initiated Crystallization of Iron–Carbon Films

S. M. Zharkov and L. I. Kveglis

Kirensky Institute of Physics, Siberian Division, Russian Academy of Sciences, Akademgorodok, Krasnoyarsk, 660036 Russia
e-mail: zharkov@iph.krasn.ru

Received September 15, 2003

Abstract—A structure formed in nanocrystalline iron–carbon films exposed to an electron beam was studied. Explosive crystallization (EC) with the formation of dendrite and cellular–dendritic instabilities at a rate of up to 1 cm/s was observed. It was shown that the dependence between the growth rate of dendrite branches (or cells) during EC and the rounding radius of dendrite branch tips can be approximately described by equations used to calculate the crystal growth in supercooled melts. To explain the EC mechanism, a model of a liquid zone formed at the crystallization front was used. It was shown that the liquid zone arises due to energy accumulated in the film in the nanocrystalline state. It was assumed that this energy was accumulated due to the energy of elastic stresses. © *2004 MAIK "Nauka/Interperiodica".*

1. INTRODUCTION

Materials with nanocrystalline structure have unique physical properties and are objects of close attention [1]. A nanocrystalline material represents a specific state of condensed matter with a high degree of nonequilibrium. The problem of thermal stability of the nanocrystalline state during crystallization under exposure to uniform or local heating is very interesting and important from both theoretical and practical viewpoints. Under conditions of a rather weak heat dissipation, crystallization can become self-enhanced. An intense release of latent heat causes significant self-heating of the crystallization front, which takes on the form of a thermal domain moving with a velocity of up to a few tens of meters per second. In this case, a liquid zone can be formed at the crystallization front. The crystallization of a sample under such conditions is generally referred to as explosive crystallization [2].

Explosive crystallization (EC) was first observed in amorphous germanium. Crystallization initiated by pulsed laser beams [3], thermal heating [4], and mechanical impact [5] have been studied. EC caused by a pulsed laser beam has been observed in amorphous (In, Ga)Sb films. Pulses with a duration of ~10^{-7} s form local polycrystalline regions in amorphous films (with a velocity of up to 5 m/s) [6]. In [7–9], EC initiated by an electron beam was observed in amorphous Fe–Ni, Dy–Co, Pr–Ni, and Fe films. As a result of crystallization, various dendrite structures were formed.

The type of instabilities arising at the phase interface during crystallization changes depending on the conditions of the process. If the crystallization front velocity is low and the heat dissipation is ideal, the crystallization front will be "smooth." In the case of steady growth in a supercooled melt, any bulges in the crystallization front should disappear, thus maintaining the smoothness of the front. In the case of unsteady growth, an increase in the degree of supercooling causes instabilities in the smooth crystallization front, characteristic of crystallization from the melt: small-scale sinusoidal perturbations of the Mullins–Sekerka type, dendritic instabilities, a cellular structure of the front [10], and fractal clusters described by the Witten–Sander model [11, 12]. The mechanisms for the formation of various instabilities during crystal growth were considered by Langer [10, 13].

This study is devoted to the crystallization of nanocrystalline iron–carbon films initiated by an electron beam in a transmission electron microscope. We analyze the dependence of the parameters of a microstructure formed during crystallization on the rate of crystallization. Studies of dendrite structures formed by annealing films in vacuum in films grown using the same technology [14–16], of the fractal oxidation of such films in air under pulsed laser beams [17], and of EC under an electron beam [18] have already been reported.

2. EXPERIMENTAL

Iron–carbon films with a carbon content of ~20 at. % were grown through pulsed-plasma evaporation in vacuum (10^{-6} Torr) onto various substrates (NaCl, MgO, LiF). The growth method is described in [16, 19]. The chemical composition was determined using Auger spectroscopy. The film thickness was 20–50 nm. The film microstructure and phase composition were studied using a PRÉM-200 transmission electron microscope, as well as by x-ray diffraction methods using x-ray synchrotron radiation (λ = 1.7482 Å). The films were separated from substrates in water or a fluoric acid solution and were placed onto electron-microscopic object-supporting grids. Crystallization in the films was initiated by an electron beam in the transmission elec-

1063-7834/04/4605-0969$26.00 © 2004 MAIK "Nauka/Interperiodica"

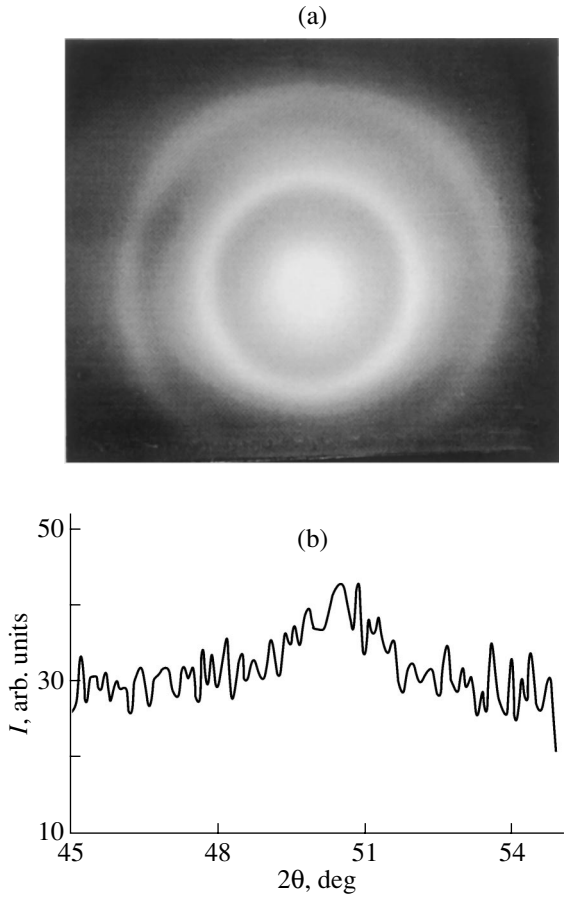

Fig. 1. (a) Electron diffraction pattern and (b) x-ray diffraction pattern obtained from an iron–carbon film in the initial state.

tron microscope in the mode of electron microscopy studies at an accelerating voltage of 125 kV and a beam current of 50–75 μA.

3. EXPERIMENTAL RESULTS

Electron diffraction patterns obtained from iron–carbon films in the initial state represent diffuse halos (Fig. 1a). In this case, the first diffraction reflection has a much higher intensity than the others. This fact suggests that the films under study are characterized by a nanocrystalline structure. The x-ray studies detect only one strongly broadened reflection (Fig. 1b). The x-ray diffraction peak broadening ($\Delta 2\theta$) is 2°–3° for various samples.

During electron microscopy studies, explosive crystallization was observed to occur in some films exposed to an electron beam. It is worth noting that the power of the electron beam incident on a sample corresponded to conventional conditions of electron microscopy studies. The crystallization rate determined visually during the studies varied from sample to sample and reached 1 cm/s. The typical electron microscopy image of the

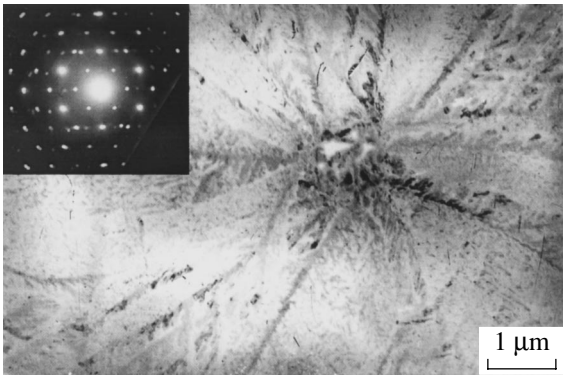

Fig. 2. Electron microscopy image of a dendrite crystal formed under an electron beam in the initial iron–carbon film. The inset shows an electron microdiffraction pattern obtained from a single dendrite branch.

film after such crystallization is shown in Fig. 2. The crystallization proceeded as follows. Initially, a crystallization center arose, from which dendrite-structure branches began to propagate in different directions. These branches, in turn, initiated new crystallization centers. The branch propagation velocity for the structure shown in Fig. 2 was ~0.25 cm/s. Due to crystallization, the film was in part covered with dendrite structures. The inset to Fig. 2 shows an electron diffraction pattern obtained by microdiffraction from a single dendrite branch. The electron diffraction pattern is spot-type and corresponds to none of the known structures of pure iron and iron–carbon compounds. The diffraction reflections in electron diffraction patterns obtained from noncrystalline film regions represented diffuse halos, as before.

In the case when it was impossible to achieve EC in the initial state, films were annealed in vacuum at T_{ann} = 100–150°C for 30 min. The electron diffraction patterns obtained from films after annealing did not differ from the electron diffraction patterns for the films in the initial state (Fig. 1a). Such films were again exposed to an electron beam, which as a rule caused crystallization. An electron microscopy image of a film after such crystallization is shown in Fig. 3. The inset to Fig. 3 shows the electron diffraction pattern obtained by microdiffraction from a single cell. The crystallization process was as follows. Initially, cells in the film grew at a rate of ~0.01 cm/s (Fig. 3, left). Then, secondary dendritic instabilities arose and developed. As a result, the film was covered in part by dendrite structures (Fig. 3, right) analogous to those observed during the crystallization of Fe–Ni films from a melt [20]. Eventually, the cellular structure was broken due to the development of secondary dendritic instabilities.

Figure 4 shows an electron microscopy image of the structure formed after a mechanical impact. An electron diffraction pattern (see inset to Fig. 4) obtained by microdiffraction from an area of ~0.5 μm shows spot reflections arranged similarly to those shown in Fig. 3.

Finally, one more group of films was observed. EC did not arise in them either in the initial state or after annealing at T = 100–150°C. However, crystallization began in such films after 5–10 min of exposure to an electron beam (at an accelerating voltage of 125 kV and a beam current of 50–75 μA, with the condenser aperture removed). The rate of this crystallization is low; as a result, a structure consisting of particles 30–150 nm in size is formed. Figure 5 shows an electron microscopy image of the structure formed after a 15 min of exposure to an electron beam. The electron diffraction pattern (see inset to Fig. 5) obtained by microdiffraction from an area of ~0.5 μm contains many randomly arranged spot reflections in place of diffuse halos.

4. DISCUSSION

If we assume that a diffraction peak in an x-ray pattern (Fig. 1b) is broadened only due to the size effect, then the size of crystallites composing the film in the initial state can be calculated using the Scherrer formula [21]

$$\Delta 2\theta = \frac{\lambda}{L\cos\theta_0}, \quad (1)$$

where $\Delta 2\theta$ is the diffraction peak width (in radians), λ is the x-ray wavelength (Å), θ_0 is the diffraction angle (deg), and L is the crystallite size (Å). At $\Delta 2\theta = 3°$, $\lambda = 1.7482$ Å, and $\theta_0 = 25°$, the largest crystallite size is ≈37 Å. This confirms the assumption of the nanocrystalline film structure based on the analysis of the intensity of diffraction reflections in an electron diffraction pattern (Fig. 1a).

We note that nonexplosive crystallization (Fig. 5) is caused by 15-min electron-beam heating and forms a structure consisting of unordered microcrystallites. This is confirmed by the randomly arranged spot reflections in the electron diffraction pattern (see inset to Fig. 5). In the case of EC, the process lasted a time of the order of a second or shorter. However, dendrite (Fig. 2) or cellular (Fig. 3) structures consisting of coherently oriented microcrystallites formed in this case. This is demonstrated by the spot electron diffraction patterns with regularly arranged reflections (see insets to Figs. 2, 3). The crystallization rate and the character of the structure formed by slow crystallization (Fig. 5) can be explained in terms of diffusion [22]. However, this mechanism cannot explain the formation of dendritic (Fig. 2) or cellular (Fig. 3) instabilities, let alone the EC rate. The values of diffusivity known for nanocrystalline materials are very large (~10^{-6} cm^2/s) [1]. However, according to [23], this can permit a growth rate of no higher than 0.2 μm/s, which is lower than the values observed in this study by a few orders of magnitude.

The character of the dendritic (Fig. 2) and cellular–dendritic (Fig. 3) structures observed after EC of nanocrystalline iron–carbon films corresponds to crystal growth in a supercooled melt [10, 13, 24]. As men-

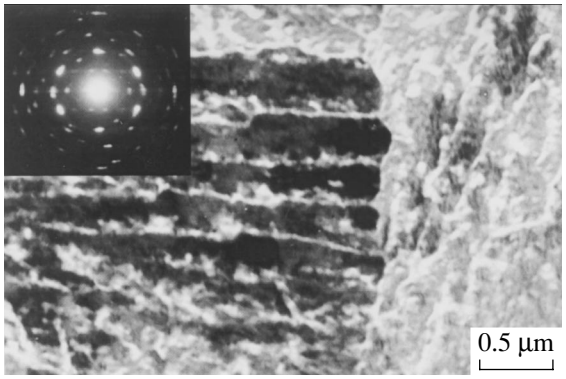

Fig. 3. Electron microscopy image of a cellular–dendritic structure formed under an electron beam in an iron–carbon film annealed in vacuum (T_{ann} = 100°C). The inset shows an electron microdiffraction pattern obtained from a single cell.

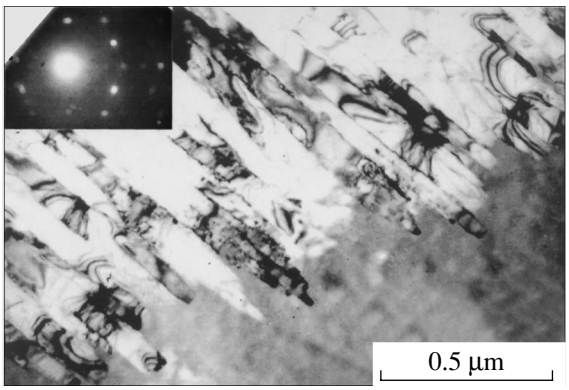

Fig. 4. Electron microscopy image of a structure formed in the initial iron–carbon film under mechanical impact. The inset shows an electron microdiffraction pattern obtained from a single cell.

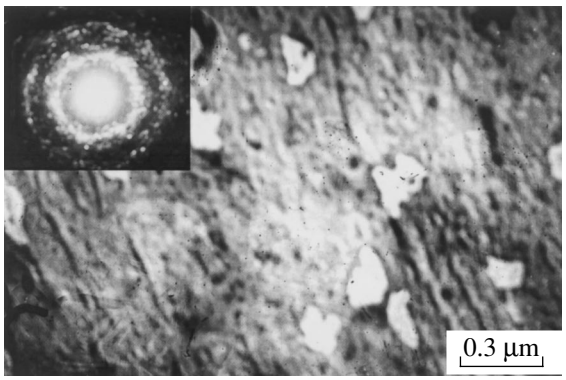

Fig. 5. Electron microscopy image of a structure formed in the initial iron–carbon film under an electron beam in 15 min. The inset shows an electron microdiffraction pattern obtained from an area of ≈0.5 μm.

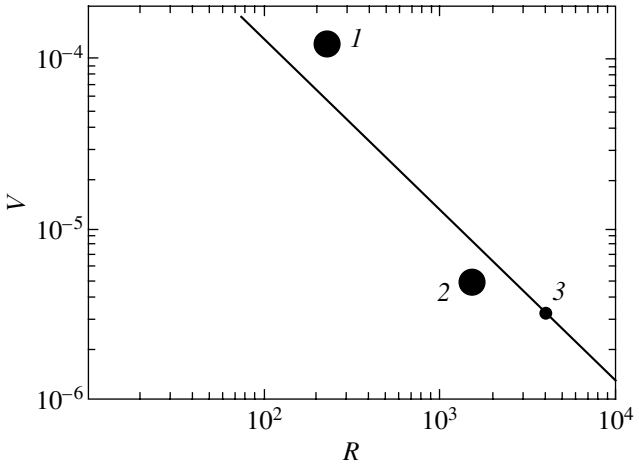

Fig. 6. Dimensionless growth rate V of a crystal in a supercooled melt vs. the rounding radius R of the crystalline needle tip [10]. The solid line corresponds to calculation [10] based on the Ivantsov equation. (*1*, *2*) The data for iron–carbon films with the structures shown in Figs. 2 and 3, respectively, studied in this work, and (*3*) the experimental result obtained in [10].

tioned above, EC can be accompanied by the formation of a liquid phase moving ahead of the crystallization front [2, 7]. The liquid phase can initiate various instabilities, including dendritic and cellular instabilities characteristic of crystallization from a melt.

As was shown by Ivantsov [25], the steady-state shape of a crystalline needle growing in a supercooled melt is a paraboloid of revolution. At a certain rounding radius $r = r_0$ of the needle tip, the growth rate of a needle will be highest. Experimentally, as the degree of supercooling ($T_{k,\infty} - T_0$) increases ($T_{k,\infty}$ is the temperature of the needle surface, T_0 is the melt temperature), the growth rate increases and the needle thickness decreases. A needle having the tip rounding radius r_0 and moving with the maximum possible velocity v_{max} at a given supercooling ($T_{k,\infty} - T_0$) will be most stable. Indeed, if a hill arises at the needle tip, it will gradually disappear, since its growth rate will be always lower than v_{max}; hence, the needle will retain its initial shape. Thus, it would be expected that the most probable needle shape will be that which provides its maximum growth rate. Figure 6 shows the dependence of the growth rate on the rounding radius of the tip of a crystalline needle growing in a supercooled melt calculated in [10] from the Ivantsov equation. Instead of the term "crystalline needle," we will use the terms "dendrite branch" and "cell." Based on the experimental data obtained in this study of the EC of nanocrystalline iron–carbon films, one can estimate the dimensionless rate V of dendrite or cellular growth and the dimensionless rounding radius R of the tip of a dendrite branch or cell: $V = v d_0/2D$ and $R = r/d_0$, where v is the growth rate of the dendrite branch or cell (cm/s), d_0 is the capillary length (~10^{-8} cm), D is the diffusivity (~10^{-5} cm^2/s), and r is the rounding radius of the tip of a dendrite branch or a cell (cm). The value of the capillary length d_0 is taken from [10], and the diffusivity D typical of molten metals is taken [26]. The dependences shown in Fig. 6 were constructed for the dimensionless supercooling $\Delta = (T_m - T)C_p/Q = 0.05$, where T_m is the melting point, T is the temperature of the supercooled melt, C_p is the specific heat, and Q is the latent heat.

By calculating the values of the dimensionless parameters V and R that correspond to our experimental data and plotting them in Fig. 6, we can approximately estimate to what extent the equations describing crystallization in the supercooled melt fit the EC processes in the films under study. The dendrite structure shown in Fig. 2 is characterized by the parameters $v \approx 0.25$ cm/s and $r = 15$–25 nm. For the cellular structure shown in Fig. 3, $v \approx 0.01$ cm/s and $r = 100$–160 nm. For the dendrite structure shown in Fig. 2, in the case of the maximum rounding radius $r = 2.5 \times 10^{-6}$ cm ($R = 250$) of the dendrite branch tip, $V = 1.25 \times 10^{-4}$ (circle *1* in Fig. 6). For the cellular structure shown in Fig. 3, at the maximum rounding radius $r = 1.6 \times 10^{-5}$ cm ($R = 1600$) of the cell tip, $V = 5 \times 10^{-6}$ (circle *2* in Fig. 6). We can see that the experimental values (Fig. 6) determined in this study are close to the curve calculated from the Ivantsov equation. Apparently, the dependence between the growth rate and the rounding radius of the tip of a dendrite branch (or a cell) for EC in the films under study can be approximately described by the formula obtained for the case of crystalline needle growth in a supercooled melt.

To find the dependences corresponding to this experiment, we need to know exact values of the quantities entering the equations (the capillary length, diffusivity, degree of supercooling, specific heat, latent heat, etc.). Accurate determination of these values is a separate intractable problem, since these characteristics nonlinearly depend on many parameters, such as the temperature gradients over the film surface, film thickness, and structural and concentration nonuniformities.

According to the estimations carried out, the local temperature of the films caused by an electron beam when initiating EC in nanocrystalline iron–carbon films was not higher than 200–250°C. The structures formed during EC are similar to those observed after annealing films in vacuum at T_{ann} = 300°C [14–16] or after mechanical impacts. Hence, the initiation of EC in the films under study requires a much lower energy than is required to melt the film [15]. The fact that the experimental results agree qualitatively with the dependences characteristic of crystal growth in the supercooled melt suggests that there is a liquid zone at the crystallization front. This zone provides conditions for the occurrence of dendritic and cellular instabilities. It is clear that the zone arose due to the release of energy stored in the film in the initial state. This energy should be at least sufficient for melting (surface melting [27, 28] or quasi-melting [29]) of nanocrystalline particles composing the film.

The mechanism for EC in the films under study is presumably as follows. An electron beam generates crystallization centers. A liquid zone arises at the front of crystallization; then, crystallization propagates over the film in the self-maintaining (autowave) mode. This mode is characterized by a release of the energy accumulated in the film during crystallization at the interface of two (solid and liquid) phases. During EC, nanoparticles that are molten on their edges aggregate with each other and form dendrite or cellular structures. Such structures exhibit scale invariance and, while having no translation symmetry, allow the formation of spot electron diffraction patterns. The crystallization model proposed can explain the fact that the dendrite (or cellular) structures, which caused spot electron diffraction patterns similar to those characteristic of single crystals, are formed from a structurally unordered nanocrystalline state in such a short time. The spot reflections in the electron diffraction pattern (Fig. 2) are distinct enough, which suggests that the crystal structure grown is perfect.

It is known that the EC front velocity reaches 1–50 m/s in some samples. However, impurity atoms in a material can decrease the crystallization rate by orders of magnitude [2]. The highest EC rates are observed in pure materials or in materials with low impurity contents (1–2 at. %). The crystallization rate of the films studied does not exceed 1 cm/s. These films contain ~20 at. % carbon, which explains the relatively low EC rates. It is most probable that a fraction of the carbon atoms in the initial state are at the surface of iron nanoparticles [15, 16]; carbon also enters into the composition of interstitial solid solutions, which do not form in the iron–carbon system in the equilibrium state [14–16].

As shown in [30, 31], the films are characterized by strong oriented and unoriented stresses, which can exceed the ultimate strength of a material in a bulk state. The strength of metal films is generally associated with their highly imperfect structure and can exceed the strength of the corresponding bulk materials by several times. As is known [32], structurally nonequilibrium regions in amorphous and nanocrystalline samples differ in energy from the thermodynamic equilibrium state by a "stress energy" with characteristic values of 5–20 kJ/mol. This energy is sufficient for a liquid zone to arise during the structural rearrangement caused by EC. It can be assumed that an energy of the same order of magnitude is accumulated in the nanocrystalline iron–carbon films under study. An argument in favor of this assumption can be a large number of bending extinction contours in an electron microscopy image (Fig. 4). The bending contours indicate bending of atomic planes caused by internal stresses. The lattice curvature radius calculated by analyzing the bending contours [33] is ≈1 μm. A comparison of the electron diffraction patterns shown in Figs. 3 and 4 shows that the atomic order formed during crystallization due to a mechanical impact (Fig. 4) is analogous to that formed by crystallization under an electron beam (Fig. 3).

The degree of nonequilibrium of nanocrystalline films (i.e., the energy accumulated in them) is controlled by technological conditions during their growth. Under nonequilibrium and nonuniform conditions, crystallization can bring about the formation of different (dendritic and cellular) structures in various films and even in a single film. These structures grow with different rates in various films. The crystallization rate is controlled by the degree of melt supercooling at the EC front and, hence, by the energy accumulated in the film. Determination of the degree of supercooling and the accurate latent heat is a separate complex problem. However, it is clear that, in films that accumulate large energy due to the technological conditions of their growth, the EC proceeds at a higher rate, requires a lower initiating energy, and results in the formation of dendrite structures (Fig. 2). In films that accumulate small energy, the crystallization initiation requires a larger energy and the process occurs at a lower rate with the formation of cellular structures (Fig. 3). In films that accumulate still smaller energy, crystallization is observed only after prolonged heating by an electron beam, is nonexplosive, and is not accompanied by the formation of cellular–dendrite structures. Finally, in equilibrium samples, crystal growth is impossible under an electron beam of such power.

The formation of dendrite and cellular instabilities during EC is a telling illustration for self-organization processes in nonequilibrium systems [34]. These instabilities occur especially often far from the equilibrium state under conditions of increasing instability of such systems. One should distinguish between the organization and self-organization phenomena; the latter is a spontaneous structurization process that occurs in an open nonequilibrium system and proceeds due to internal energy sources of the system itself, whereas the organization processes occur due to external energy sources. In the case under consideration, nonexplosive crystallization is caused by an electron beam (i.e., an external energy source) and corresponds to organization. EC is an example of self-organization, since the EC process (although initiated by an electron beam) occurs due to the energy accumulated in the film.

5. CONCLUSIONS

Thus, this study has shown that both ordinary and explosive crystallizations can take place in nanocrystalline iron–carbon films under an electron beam. The EC process occurs at a rate of up to 1 cm/s with the formation of dendritic or cellular–dendritic instabilities. Electron diffraction patterns obtained from films after EC are spot-type and do not correspond to any of the known structures of either pure iron or iron–carbon compounds. The crystallization model proposed explains the fact that the structures with spot-type electron diffraction patterns (similar to those characteristic of single crystals) are formed from a structurally unordered nanocrystalline state in such a short time.

The relation between the growth rate of dendrite branches (or cells) during EC and the rounding radius of the tip of a dendrite branch or a cell was approximately described by equations derived for the crystal growth in a supercooled melt. The following feature characteristic of crystallization in a supercooled melt was established: the higher the growth rate, the lower the rounding radius of the dendrite branch (or cell) tip. This allows us to conclude that EC in the films under study proceeds with the formation of a liquid phase at the crystallization front. The liquid zone arises due to the energy accumulated in the film in the nanocrystalline state rather than as a result of external exposure. It was assumed that crystallization under an electron beam is controlled by the energy accumulated in the film in the initial state.

ACKNOWLEDGMENTS

The authors are grateful to V.S. Zhigalov for putting the samples at their disposal and for his assistance in the experiment, S.V. Mytnichenko and A.V. Bessergenev for their assistance in the x-ray diffraction studies, V.G. Kesler for the study of the film chemical composition, and V.G. Myagkov for helpful discussions.

This study was supported by the Russian Foundation for Basic Research (project nos. 00-02-17358a, 03-02-16052a), the sixth competition of the Examination of Scientific Projects of Young Scientists of the Russian Academy of Sciences (1999, project no. 56), and INTAS (grant no. 00-100).

REFERENCES

1. H. Gleiter, Prog. Mater. Sci. **33**, 223 (1989).
2. V. A. Shklovskiĭ and V. M. Kuz'menko, Usp. Fiz. Nauk **157** (2), 311 (1989) [Sov. Phys. Usp. **32**, 163 (1989)].
3. R. Messier, T. Takamori, and R. Roy, Solid State Commun. **16** (3), 311 (1975).
4. R. Koba and C. E. Wickersham, Appl. Phys. Lett. **40** (8), 672 (1982).
5. A. Mineo, A. Matsuda, T. Kurosu, and M. Kikuchi, Solid State Commun. **13** (9), 1307 (1973).
6. C. E. Wickersham, G. Bajor, and J. E. Greene, Solid State Commun. **27** (1), 17 (1978).
7. O. Bostanjoglo and R. Liedtke, Phys. Status Solidi A **60** (2), 451 (1980).
8. V. G. Myagkov, L. I. Kveglis, and G. I. Frolov, Poverkhnost, No. 9, 131 (1992).
9. V. G. Myagkov, L. I. Kveglis, V. S. Zhigalov, and G. I. Frolov, Poverkhnost, No. 1, 105 (1994).
10. J. S. Langer, Rev. Mod. Phys. **52** (1), 28 (1980).
11. T. A. Witten and L. M. Sander, Phys. Rev. Lett. **47** (19), 1400 (1981).
12. B. M. Smirnov, Usp. Fiz. Nauk **149** (2), 177 (1986) [Sov. Phys. Usp. **29**, 481 (1986)].
13. J. S. Langer, Science **243**, 1150 (1989).
14. S. M. Zharkov, V. S. Zhigalov, L. I. Kveglis, Yu. V. Lisitsa, K. V. Renskaya, and G. I. Frolov, Pis'ma Zh. Éksp. Teor. Fiz. **65** (12), 872 (1997) [JETP Lett. **65**, 915 (1997)].
15. S. M. Zharkov, Candidate's Dissertation (Inst. of Physics, Siberian Division, Russian Academy of Sciences, Krasnoyarsk, 1999).
16. G. I. Frolov, V. S. Zhigalov, L. I. Kveglis, S. M. Zharkov, O. A. Bayukov, and A. L. Bas'ko, Fiz. Met. Metalloved. **88** (2), 85 (1999).
17. V. G. Myagkov, V. S. Zhigalov, and S. M. Zharkov, Dokl. Akad. Nauk **346** (2), 612 (1996) [Phys. Dokl. **41**, 55 (1996)].
18. S. M. Zharkov and L. I. Kveglis, Dokl. Akad. Nauk **383** (5), 617 (2002) [Dokl. Phys. **47**, 281 (2002)].
19. V. S. Zhigalov, G. I. Frolov, and L. I. Kveglis, Fiz. Tverd. Tela (St. Petersburg) **40** (11), 2074 (1998) [Phys. Solid State **40**, 1878 (1998)].
20. W. J. Boettinger, S. R. Coriell, A. L. Greer, A. Karma, W. Kurz, M. Rappaz, and R. Trivedi, Acta Mater. **48** (1), 43 (2000).
21. A. Guinier, *Theórie et Technique de la Radiocristallographie* (Dunod, Paris, 1956; Fizmatgiz, Moscow, 1961).
22. L. N. Paritskaya, Poroshk. Metall. (Kiev), No. 11, 44 (1990).
23. Yu. I. Vesnin, *Secondary Structure and Properties of Crystals* (Inst. Neorg. Khim. Sib. Otd. Ross. Akad. Nauk, Novosibirsk, 1997).
24. W. Kurz and D. J. Fisher, *Fundamentals of Solidification* (Trans. Tech., Switzerland, 1986).
25. G. P. Ivantsov, Dokl. Akad. Nauk SSSR **58** (4), 567 (1947).
26. *Physical Quantities. Handbook*, Ed. by I. S. Grigor'ev and E. Z. Meĭlikhov (Énergoatomizdat, Moscow, 1991).
27. A. Trayanov and E. Tosatti, Phys. Rev. Lett. **59** (19), 2207 (1987).
28. J. W. M. Frenken, P. M. J. Marée, and J. F. van der Veen, Phys. Rev. B **34** (11), 7506 (1986).
29. P. M. Ajayan and L. D. Marks, Phys. Rev. Lett. **63** (3), 279 (1989).
30. M. Ya. Fuks, Izv. Akad. Nauk SSSR, Ser. Fiz. **31** (3), 422 (1967).
31. V. A. Buravikhin, *Influence of Mechanical Stresses on the Magnetic Properties of Films* (Vost.-Sib. Kn., Irkutsk, 1968).
32. S. F. Timashev and L. I. Trakhtenberg, Zh. Fiz. Khim. **67** (3), 448 (1993).
33. V. Yu. Kolosov and A. R. Thölen, Acta Mater. **48** (8), 1829 (2000).
34. G. Nicolis and I. Prigogine, *Self-Organization in Non-Equilibrium Systems* (Wiley, New York, 1977; Mir, Moscow, 1979).

Translated by A. Kazantsev